Indonesian Physical Review
Volume 08 Issue 03, September 2025
P-ISSN: 2615-1278, E-ISSN: 2614-7904

Sea-Level Variability in the Java Sea Linked to Monsoon Forcing and Climate Teleconnections (2009–2024)

Imma Redha Nugraheni[1*], Tri Anggun Lestari[2], Aries Kristianto[1], Avrionesti[1], Hasti Amrih Rejeki[3], Yusuf Jati Wijaya[4]

[1]*Department of Meteorology, State College of Meteorology, Climatology, and Geophysics (STMKG), Indonesia*
[2]*Center for Space and Remote Sensing Research, National Central University, Taiwan*
[3]*Department of Marine Sciences and Technology, Faculty of Fisheries and Marine Science, IPB University, Indonesia*
[4]*Department of Oceanography, Faculty of Fisheries and Marine Science, Diponegoro University, Indonesia*

Corresponding Author's E-mail: imma.redha@stmkg.ac.id

Article Info

Article info:
Received: 03-09-2025
Revised: 11-09-2025
Accepted: 24-09-2025

Keywords:
Java Sea; sea level; DUACS altimetry; ENSO; IOD

How To Cite:
I. R. Nugraheni, T. A. Lestari, A. Kristianto, Avrionesti, H. A. Rejeki, and Y. J. Wijaya. "Sea-Level Variability in the Java Sea Linked to Monsoon Forcing and Climate Teleconnections (2009–2024)", Indonesian Physical Review, vol. 8, no. 3, p 790-803, 2025.

DOI:
https://doi.org/10.29303/ipr.v8i3.571.

Abstract

The Java Sea is a shallow, strait-connected shelf where seasonal monsoon forcing and climate modes can strongly modulate sea level, yet their sectoral expressions remain under-resolved. Altimetric observations from 2009–2024 (DUACS) are analyzed and validated against a network of Indonesian tide gauges and partition the basin into western (W-JS), central (C-JS), and eastern (E-JS) sectors. After detrending, the seasonal cycle is diagnosed via amplitude and phase metrics and quantifies interannual teleconnections using lead–lag cross-correlations (−12 to +12 months) between sea-level anomaly (SLA) and the Dipole Mode Index (DMI) and Southern Oscillation Index (SOI), with confidence intervals. DUACS reproduces tide-gauge variability with high skill (median correlation ≈ 0.82; RMSE 5–11 cm; small negative biases), supporting its use as a basin proxy. Seasonally, SLA peaks in DJF, weakens in MAM, reaches a pronounced minimum in JJA, and recovers in SON, with marked zonal heterogeneity: E-JS exhibits the strongest annual range (~18 cm) versus W-/C-JS (~12–13 cm). The seasonal phase is non-synchronous (W-JS maxima in May–June; E-JS in December–January), while C-JS behaves as a transition zone. Interannually, IOD impacts are near-synchronous and negative (lag-0, r ~ −0.41 to −0.47 across sectors), whereas ENSO peaks at short positive lags (SOI leads by ~1 month; r ~ 0.45–0.53), implying higher sea level during La Niña and lower during El Niño. These sign-and-lag relationships, combined with tide and surge information, have the potential to inform seasonal outlooks for ports and low-lying coastal areas of Java.

Copyright (c) 2025 by Author(s), This work is licensed under a Creative Commons Attribution-ShareAlike 4.0 International License.

Introduction

The Java Sea is a shallow, semi-enclosed basin within the Maritime Continent, where sea level affects navigation, fisheries, and coastal-flood risk for densely populated shorelines [1-5]. Dynamically, sea-level variability in the Java Sea is primarily governed by the Asian (Northwest)–Australian (Southeast) Monsoon and modulated by the El Niño–Southern Oscillation (ENSO) and the Indian Ocean Dipole (IOD). Seasonal reversals of the monsoon alter wind stress, pressure gradients, and circulation pathways over the shallow shelf, producing a pronounced seasonal cycle in sea level [6, 7]. At interannual time scales, phases of ENSO and the IOD modify surface winds and upper-ocean conditions across the Indonesian seas, yielding sea-level anomalies in the Java Sea with month-scale lags relative to the Southern Oscillation Index (SOI) and the Dipole Mode Index (DMI) [8, 9]. Variations in mass and freshwater exchange between the Java Sea and surrounding waters (e.g., via the Karimata Strait) further reshape density structure and sea level, highlighting the basin's sensitivity to basin-scale climate modes [10].

Despite growing attention to the roles of the monsoon and ENSO/IOD teleconnections across the Maritime Continent, consistent quantification for the Java Sea remains limited. First, basin-wide mapping of seasonal amplitude and phase, together with associated uncertainty (e.g., 95% confidence intervals), has not been synthesized across the western–central–eastern sectors [6, 7]. Second, reported lead–lag relationships with SOI/DMI vary by analysis windows and method, motivating a uniform, month-by-month evaluation [8, 9].

From a data perspective, gridded satellite altimetry from the Data Unification and Altimeter Combination System (DUACS) [11] offers continuous basin-scale coverage but faces challenges in shallow and near-coastal waters (e.g., retrieval issues and land contamination). Cross-validation against tide gauges is therefore essential to assess correlation, root-mean-square error (RMSE), and bias [12, 13]. At the same time, interpretation of coastal impacts must recognise that land subsidence in many Javanese coastal cities can dominate relative sea-level change, warranting a clear separation of oceanic variability from geotectonic/geotechnical issues [14, 15].

Addressing these gaps, the present study does not estimate long-term trends. Instead, seasonal and interannual variability of sea level in the Java Sea and its relationships with the monsoon, ENSO (via SOI), and the IOD (via DMI) is examined at monthly resolution (2009–2024). Specifically: (i) DUACS consistency is validated against available tide gauges (reporting correlation (r), RMSE, bias, and confidence intervals) to ensure reliability of the baseline dataset; (ii) climatology and seasonal amplitude and phase (2009–2024) are mapped across three sectors of the Java Sea (western–central–eastern); and (iii) ENSO/DMI linkages to Java Sea level are investigated by quantifying the lead–lag structure (−12 to +12 months) between sea level and SOI/DMI, with associated confidence intervals. Lag-0 correlations are reported for context, but primary inference relies on the cross-correlation function.

Data and Methodology

Research location

Analyses focus on the Java Sea (105–115°E, 3–9°S), a shallow, semi-enclosed shelf basin within the Maritime Continent. To diagnose longitudinal heterogeneity, the domain is partitioned into three sub-regions: W-JS (106–109°E, 3.2–6.0°S), C-JS (109–112°E, 3.5–6.3°S), and E-JS (112–

115°E, 3.8–6.6°S) (Figure 1). Unless otherwise stated, the analysis spans 2009–2024 at monthly resolution.

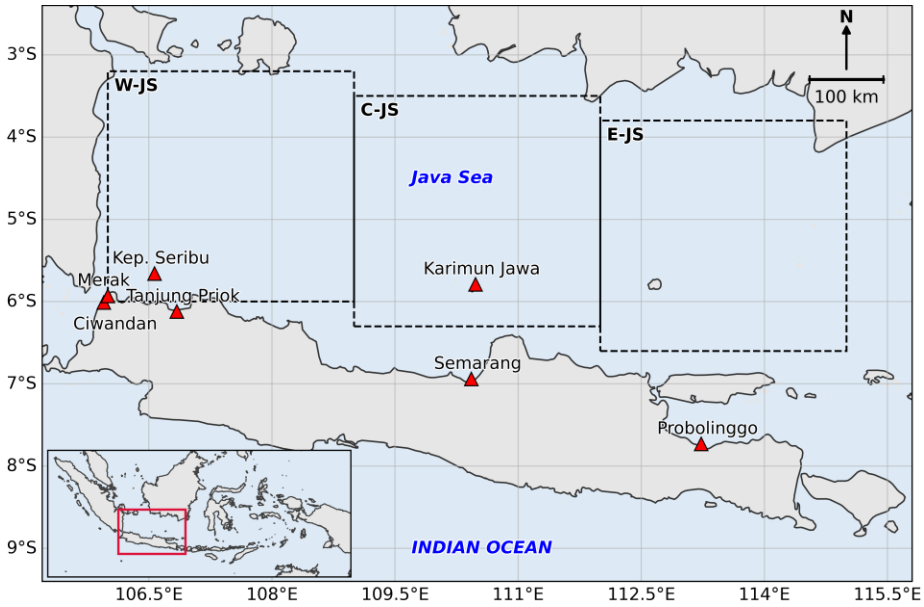


Figure 1. Study area in the Java Sea showing W-JS, C-JS, and E-JS subregions and tide-gauge stations.

Datasets

Sea level is represented using the Copernicus Marine Service (CMEMS) DUACS Level-4 multi-mission altimetry product (global physical sea level; product family SEALEVEL_GLO_PHY_L4_*, 1/4° grid) [11] to represent sea level over the basin. Daily absolute dynamic topography (ADT) fields are used on the native grid, and sea-level anomaly (SLA) is formed by removing the 2009–2024 monthly climatology from the daily ADT (i.e., anomalies about the monthly mean). Tide-gauge records at minute resolution from seven stations around the Java Sea (obtained from BMKG InaTNT) undergo standard quality control (spike/outlier removal, datum checks) and are then aggregated to daily means to attenuate tidal and other high-frequency variance outside the scope of this study. Station-specific analysis windows during 2021–2024 follow TG availability and are aligned to the DUACS daily calendar.

Two monthly climate indices are used to characterise large-scale variability: (i) the Dipole Mode Index (DMI) (the west–east SST gradient in the tropical Indian Ocean from the HadISST-based dataset curated by NOAA PSL) (https://psl.noaa.gov/data/timeseries/month/DMI/); and (ii) the Southern Oscillation Index (SOI) (a standardised sea-level pressure–based metric of ENSO from NOAA CPC) (https://www.cpc.ncep.noaa.gov/products/analysis_monitoring/ensocycle/soi.shtml). Both series were accessed on 1 Aug 2025. Positive DMI denotes a warm western/ cool eastern Indian Ocean (IOD-positive), whereas positive SOI corresponds to La Niña-like conditions.

DUACS-tide gauge validation

For each tide gauge, DUACS values are extracted from the nearest valid ocean grid cell. Skill is evaluated with Pearson correlation (r), root-mean-square error (RMSE), and bias (DUACS-TG), together with 95% confidence intervals (CI). Tide-gauge records are used solely to

validate DUACS skill and are not included in the box-mean SLA diagnostics inside the analysis polygon. Validation establishes that DUACS reliably represents daily variability in shallow/near-coastal Java Sea waters before using it as a basin proxy.

Seasonal climatology, amplitude, and phase

Monthly ADT fields for 2009–2024 are aggregated into a 12-month climatology at each grid cell. Seasons follow the meteorological convention (DJF, MAM, JJA, SON) with DJF comprising December of year *N–1* and January–February of year *N*. To summarize longitudinal structure, cosine-latitude-weighted monthly means (weight = cos φ) are computed for W-JS, C-JS, and E-JS.

Linear detrending was applied to the monthly ADT time series at each grid cell to isolate the seasonal signal from long-term changes. The procedure follows standard practice in physical oceanography and climate time-series analysis. From the detrended series, a monthly climatology was constructed by averaging identical calendar months across 2009–2024 at each grid cell. Seasonal amplitude at each location was then defined as the difference between the highest and lowest values of this 12-month climatology (reported in centimeters), and the phase as the calendar month in which the climatology reaches its annual maximum. The same definitions are applied to the three sub-regions using their weighted 12-month curves. This yields gridded maps of amplitude and phase and box-mean seasonal cycles for W-JS, C-JS, and E-JS.

SLA–climate co-variability and lead–lag relationships (cross-correlation)

To place Java Sea variability in a broader climate context, box-mean monthly normalized sea level (SLA) for W-JS, C-JS, and E-JS is related to the SOI and DMI over their common period. Linear co-variability is summarised by Pearson correlations between SLA and each index computed on the aligned monthly series, with associated 95% confidence intervals. This step provides a compact, time-consistent view of how Java Sea sea-level variability relates to ENSO and the Indian Ocean Dipole, complementing our DUACS–TG validation and the seasonal climatology, amplitude, and phase analyses.

Lead–lag structure is quantified using the cross-correlation function (CCF) between box-mean SLA (standardized) and each index for integer lags from −12 to +12 months. The sign convention is positive lag = index leads SLA. For each sector–index pair (SLA–SOI, SLA–DMI), the peak correlation, its lag, and the full lag profile are reported.

Results and Discussion

Across seven tide-gauge (TG) sites, DUACS reproduces daily sea-level anomalies with moderate-to-very strong correlations (r=0.50–0.855; median 0.817), RMSE 5–11 cm, and generally small negative biases (mean ≈ −1.8 cm) (Table 1). Skill is highest at Kepulauan Seribu, Ciwandan, and Karimunjawa, whereas Merak and Semarang show comparatively lower agreement; Tanjung Priok records the largest RMSE, consistent with the complexities of near-coastal ports and possible land-contamination effects. Probolinggo exhibits a larger negative bias (−5.8 cm), likely reflecting near-coastal retrieval challenges. Importantly, all 95% CIs for **r** exclude zero, supporting the use of DUACS as a basin-scale proxy for seasonal and interannual variability. Subsequent analyses, therefore, focus on seasonal amplitude and phase and lead–lag relations with SOI/DMI, with uncertainties reported throughout.

Table 1. DUACS–tide gauge validation by station. n = number of paired monthly observations after alignment and QC; RMSE and bias in centimeters; bias = DUACS−tide gauge. Correlations are Pearson r with 95% confidence intervals.

Site	r	n	RMSE (cm)	BIAS (cm)	r_lo95	r_hi95
Ciwandan	0.855	560	8.4	-1.8	0.831	0.876
Merak	0.500	736	10.4	-0.7	0.443	0.552
Tanjung Priok	0.605	621	11.3	-1.8	0.552	0.652
Karimunjawa	0.827	250	5.3	-0.3	0.784	0.863
Kep. Seribu	0.849	537	5.0	-1.2	0.824	0.871
Semarang	0.650	659	7.2	-1.3	0.604	0.692
Probolinggo	0.817	378	7.9	-5.8	0.780	0.848

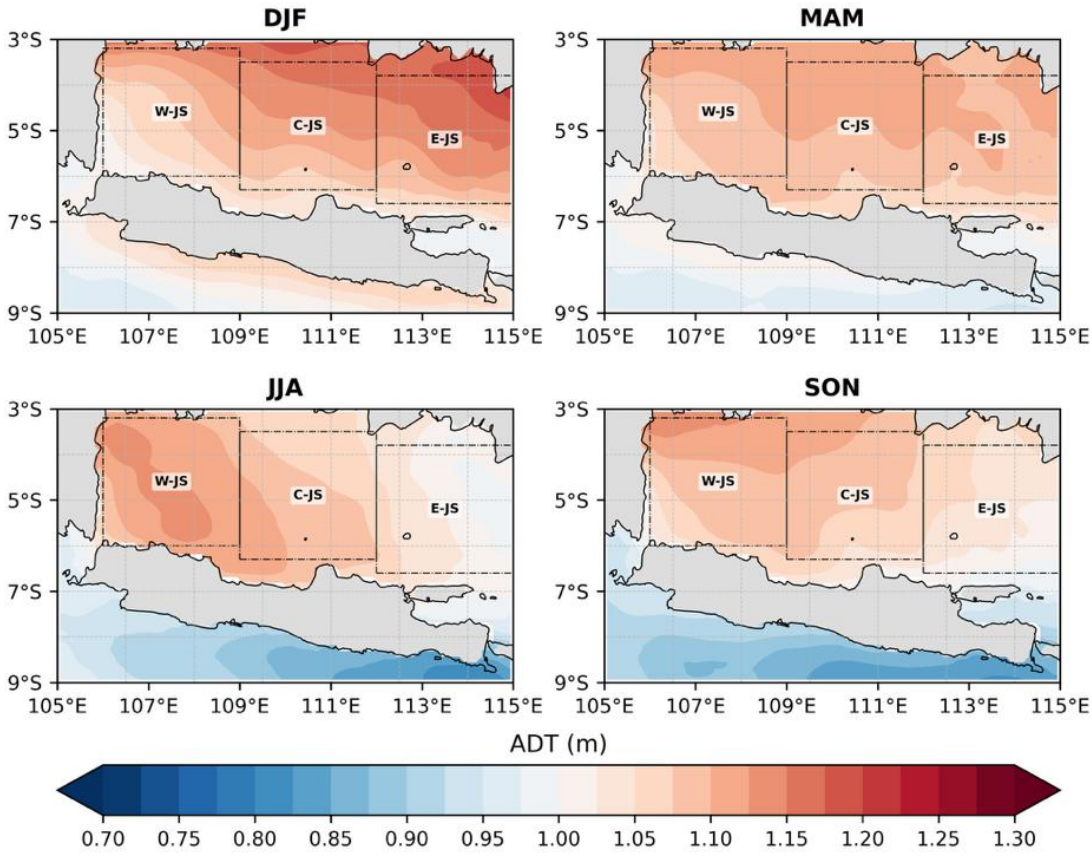


Figure 2. Seasonal climatology of absolute dynamic topography (ADT) over the Java Sea (2009–2024) and zonal heterogeneity across the three sub-regions W-JS, C-JS, and E-JS.

The seasonal climatology of absolute dynamic topography (ADT) (Figure 2) exhibits a persistent meridional gradient, with higher sea level north of Java (Java Sea) and lower sea level to the south of Java (eastern Indian Ocean). Within the Java Sea, DJF attains the highest

levels, MAM weakens while preserving the meridional contrast, JJA reaches a clear minimum (most pronounced in the eastern Java Sea (E-JS) and SON returns to intermediate values. This seasonality is consistent with monsoon forcing: Northwest Monsoon (DJF) favour an elevated setup over the shelf, whereas Australian Monsoon (JJA) favour a depressed setup. The strait and shelf connectivity (e.g., Karimata and Sunda) likely further modulates the basin pattern.

W-JS maintains relatively higher ADT year-round compared with the other sub-basins, with a clear meridional slope (higher near ~3–4°S, decreasing toward ~6°S). A tongue-like extension of elevated ADT intermittently protrudes southward along the western flank of the basin. Notably, W-JS remains comparatively resilient in JJA, retaining a pocket of elevated sea level in the west, in contrast to E-JS, which exhibits the sharpest seasonal minimum. C-JS behaves as a transition zone between the western and eastern Java Sea. It follows the basin-wide seasonal sequence (DJF high → MAM weakening → JJA relative minimum → SON recovery), but the JJA minimum is less deep than in the east, partly due to a spatial shift of the minimum and relative strengthening toward the southwest. E-JS shows the strongest seasonal contrast among the three sub-basins, with DJF peaks and a pronounced JJA minimum.

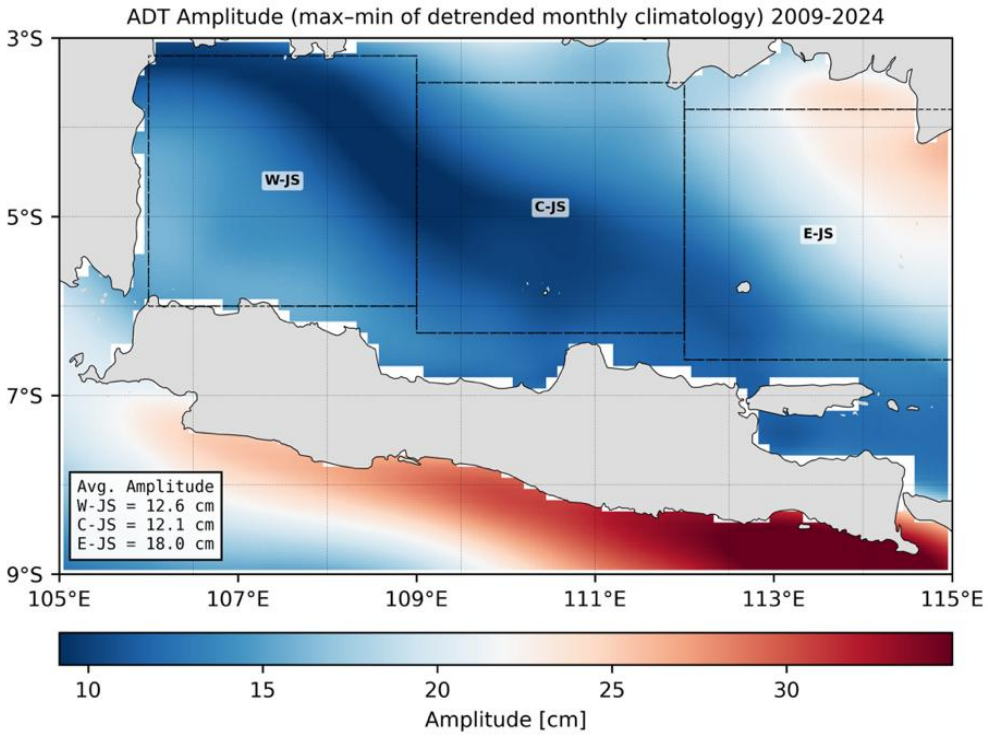


Figure 3. Seasonal amplitude of sea level (ADT; max–min of the monthly climatology, 2009–2024). Shading indicates amplitude in centimeters; the lower-left inset lists the area-weighted mean amplitude for W-JS, C-JS, and E-JS.

Figure 3 maps the seasonal amplitude, defined as the peak-to-trough range of the 12-month climatology, and summarises box-mean values for the three sub-basins. The Java Sea exhibits a weaker seasonal cycle overall (~10–25 cm), whereas waters south of Java (Indian Ocean) show substantially larger amplitudes (~25–35 cm). Within the basin, a clear west–to–east gradient emerges: W-JS and C-JS are dominated by low-to-moderate amplitudes (area-weighted means 12.1–12.6 cm), while E-JS displays a larger amplitude (mean ≈18 cm), with

maxima concentrated toward its northern and eastern flanks. This pattern is consistent with the seasonal diagnostics in Figure 2, where the JJA minimum is sharpest in E-JS, yielding the largest annual range in that sector.

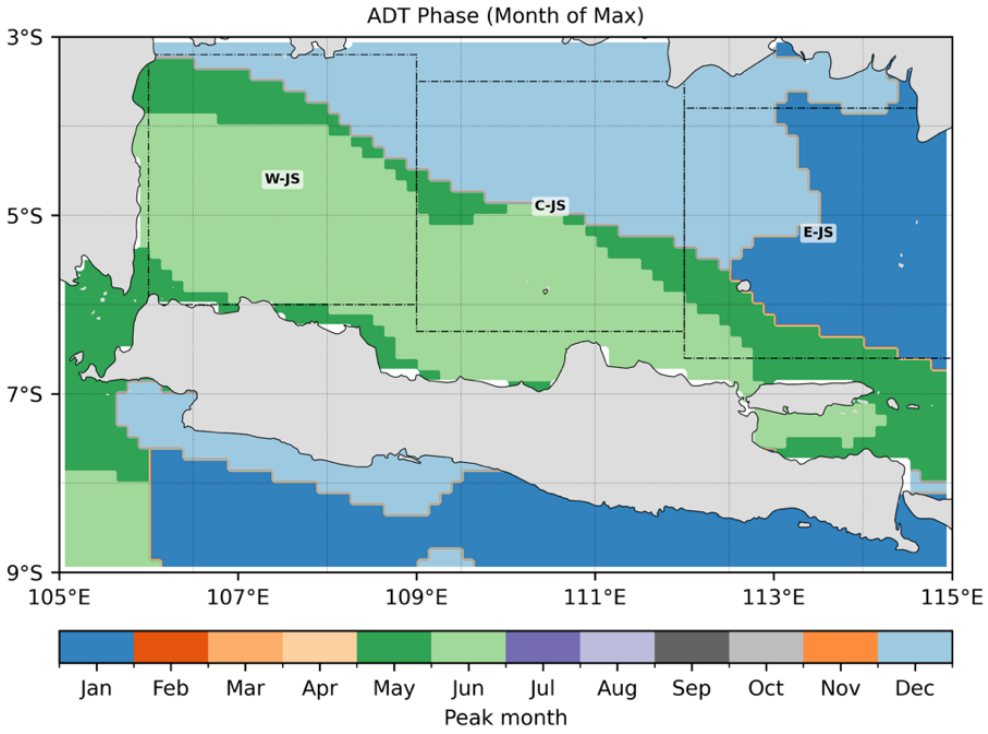


Figure 4. Seasonal phase of sea level over the Java Sea (2009–2024), defined as the calendar month of the annual maximum from the detrended monthly ADT climatology.

Figure 4 reveals a non-synchronous seasonal phase across the Java Sea, with the month of peak sea level shifting from west to east. In W-JS, peaks occur predominantly in May–June, i.e., the late transition toward the Southeast (Australian) Monsoon (JJA, prevailing easterlies). C-JS shows a transition pattern: the western and southern portions peak in May–June (onset of the Southeast Monsoon, JJA), whereas the eastern–northern sector shifts to December–January, aligned with the Northwest (Asian) Monsoon (DJF, prevailing westerlies). In E-JS, the peak occurs mostly in December–January during the Northwest Monsoon (DJF), with only a narrow southern coastal band retaining May–June maxima tied to the onset of the Southeast Monsoon (JJA). This zonally varying phasing is consistent with spatial contrasts in wind setup under these monsoon regimes and with strait/shelf connectivity.

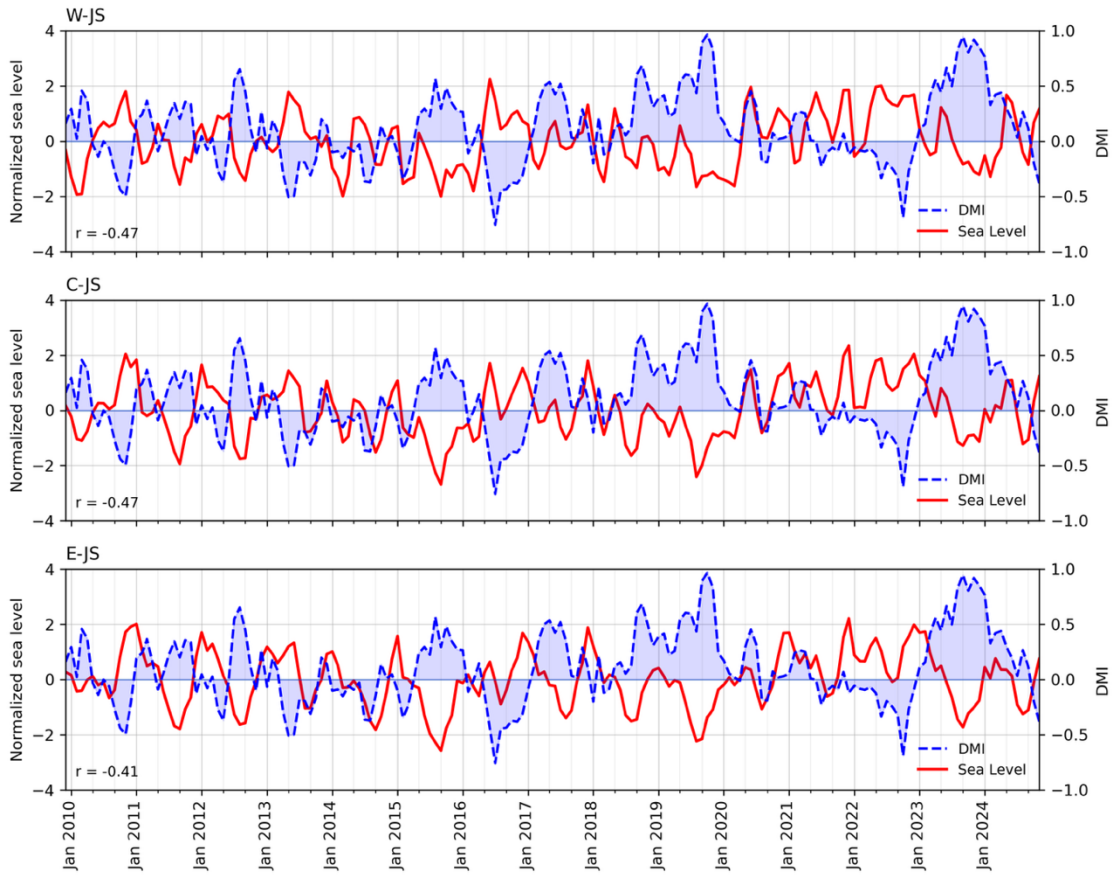


Figure 5. Time series of standardized monthly sea-level anomaly (SLA) (red, left axis) and standardized Dipole Mode Index (DMI) (blue dashed, right axis) for W-JS, C-JS, and E-JS over 2009–2024. Numbers in each panel report the lag-0 correlation (r) between SLA and DMI.

Monthly box-mean SLA (standardized) in the three Java Sea sectors covaries negatively with the standardized DMI throughout 2009–2024 (Figure 5). At lag-0, correlations are −0.47 in W-JS and C-JS, and −0.41 in E-JS, indicating that IOD-positive months are generally accompanied by below-normal sea level, whereas IOD-negative months coincide with above-normal sea level. Prominent IOD-positive episodes (late 2015–early 2016, 2019, 2023) align with basin-wide SLA minima, while IOD-negative intervals (e.g., 2010–2011, parts of 2016–2017) align with SLA maxima. The association is strongest in the western–central sectors and slightly weaker in the east, suggesting spatial heterogeneity in the basin's sensitivity.

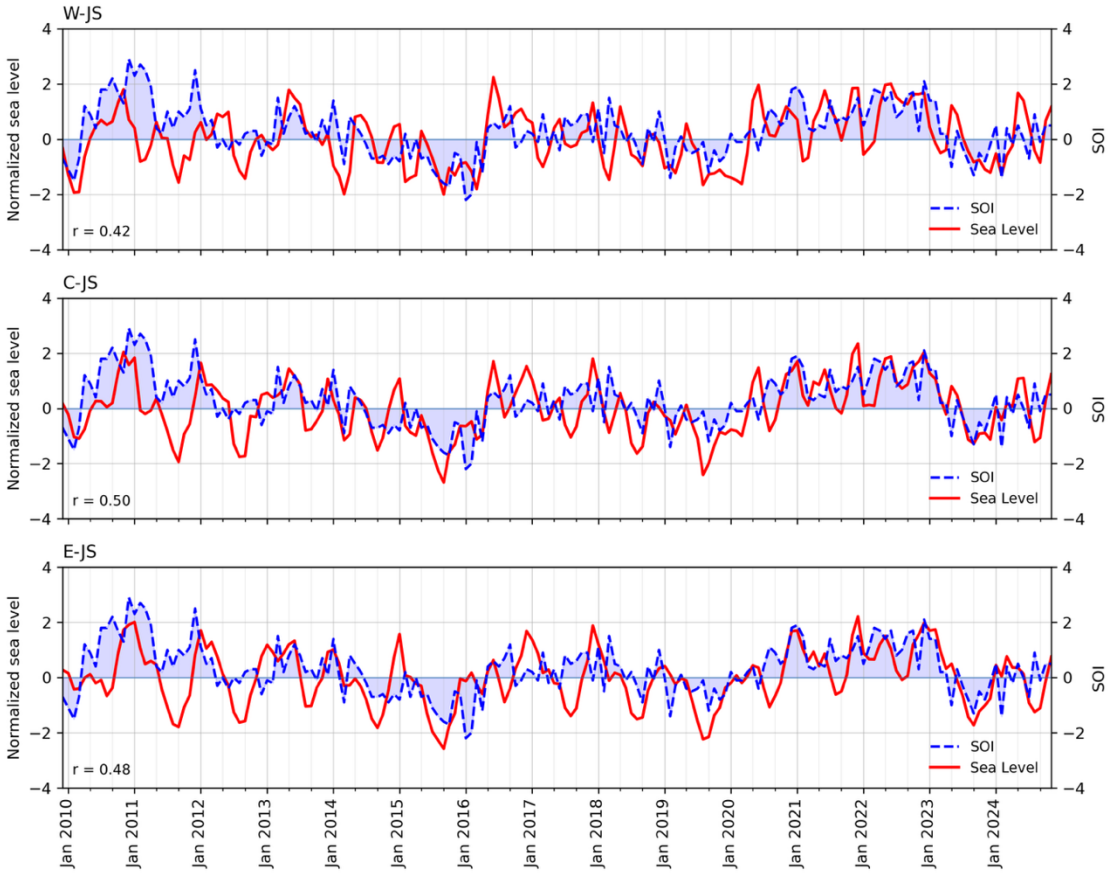


Figure 6. Time series of standardized monthly sea-level anomaly (SLA) (red, left axis) and the Southern Oscillation Index (SOI) (blue dashed, right axis) for W-JS, C-JS, and E-JS, 2009–2024. Numbers in each panel report the lag-0 correlation (r) between SLA and SOI.

Monthly SLA covaries positively with SOI across all three sectors (lag-0 $r \approx 0.42$ in W-JS, 0.50 in C-JS, 0.48 in E-JS) (Figure 6), implying higher sea level during La Niña (positive SOI) and lower sea level during El Niño (negative SOI). The co-variability is clearest during major events: La Niña 2010–2011 and the 2020–2022 "triple-dip" coincide with basin-wide SLA maxima, whereas El Niño 2015–2016 and late-2023/early-2024 align with depressed SLA. The association is strongest in C-JS and comparable in W-JS and E-JS, indicating modest west–east heterogeneity.

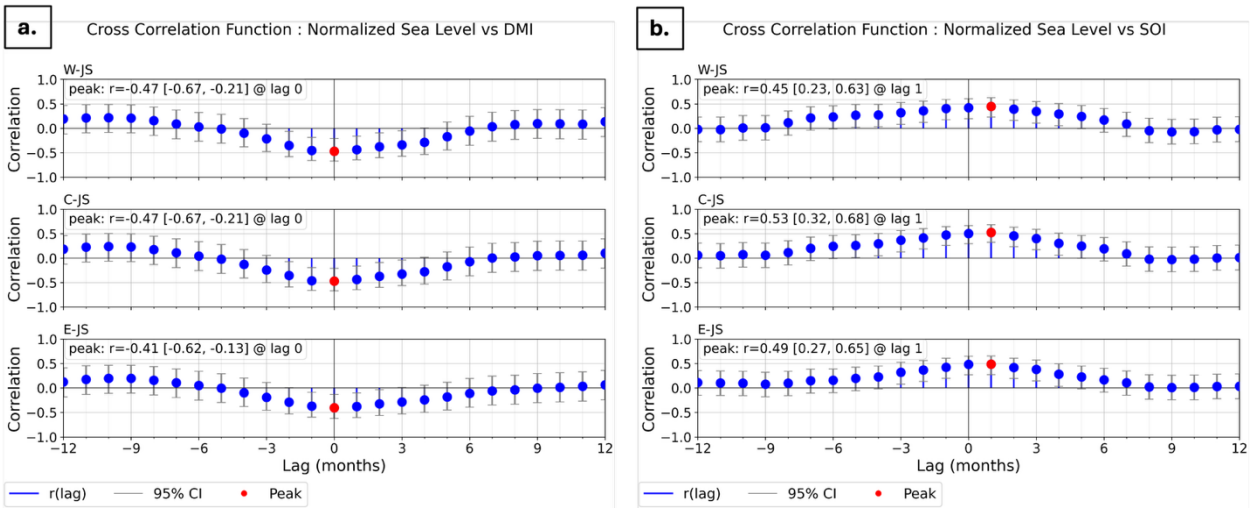


Figure 7. Lead–lag cross-correlation (−12 to +12 months) between monthly box-mean SLA (a) and DMI (b) in the Java Sea (2009–2024). Dots show r (lag) for W-JS, C-JS, and E-JS; whiskers are 95% CIs; positive lag = SLA lags the index; red dot marks the peak.

Cross-correlation analysis (−12 to +12 months; positive lags denote SLA lagging the climate index) reveals two robust signals (Figure 7a,b). First, the IOD imprint is near-synchronous: peak correlations occur at lag 0 with a negative sign in all sectors (W-JS r = −0.47 [−0.67, −0.21], C-JS r = −0.47 [−0.67, −0.21], and E-JS r = −0.41 [−0.62, −0.13]), indicating lower-than-normal sea level during IOD+ months and higher-than-normal sea level during IOD−. Away from lag 0, coefficients decay rapidly and most confidence intervals include zero, suggesting limited month-scale memory relative to DMI.

Second, the ENSO imprint is delayed by ~1 month: peak positive correlations with SOI occur at lag +1 (W-JS r = 0.45 [0.23, 0.63], C-JS r = 0.53 [0.32, 0.68], E-JS r = 0.49 [0.27, 0.65]) such that La Niña precedes elevated sea level and El Niño precedes depressed sea level by roughly one month. Correlations weaken toward zero beyond ~±4 months.
Spatially, the response is strongest in the western–central sectors and slightly weaker in the east, for both drivers. All reported peaks have 95% confidence intervals that exclude zero, supporting the inferred signs and lags.

Our results show that sea level in the Java Sea exhibits a strongly seasonal shelf response to the Northwest–Southeast Monsoon with sector-dependent amplitude and phase, and a robust interannual co-variability with the IOD and ENSO. These results extend earlier findings by providing sector-resolved diagnostics that clarify how monsoon winds and climate modes modulate hydrography and circulation across Indonesian seas, thereby influencing shelf sea level variability [16-21].

Consistent with Figure 3, a meridional contrast is evident: during JJA, southeasterly alongshore winds south of Java drive offshore Ekman transport and coastal upwelling that depresses coastal sea level along the southern margin, whereas wind stress over the shallow Java Sea promotes shelf setup to the north. The DJF reversal weakens the southern upwelling signal and elevates shelf levels; exchanges through the Sunda and Karimata Straits further modulate pressure gradients and along-shelf transport [16, 17, 22]. The basin-wide sequence (high sea level in DJF, weakening in MAM, a pronounced JJA minimum, and partial recovery

in SON) is consistent with wind setup/set-down acting over a shallow shelf. Spatial phase differences among western, central, and eastern sectors of Java Sea likely arise from coastline orientation/fetch and from exchanges with neighbouring basins via straits, which together set the timing and magnitude of local setup [16, 17]. Spatial heterogeneity across the basin is also evident in interannual studies that find east–west differences under ENSO/IOD forcing [23], [24], reinforcing the plausibility of stronger seasonal swings in the east.

Our lead–lag analysis indicates a near-synchronous IOD imprint (negative SLA during positive IOD months and vice versa) and a short-lag ENSO imprint where the index leads SLA. These timings and signs agree with documented pathways: IOD events reorganize regional winds, upwelling, and hydrographic conditions over Indonesian waters [17], while ENSO modulates the Indonesian Throughflow (ITF) and regional currents. La Niña periods are associated with increased transports and higher sea levels, and El Niño with the opposite tendency [25]. Because IOD and ENSO can co-occur, months with simultaneous anomalies are noted qualitatively; isolating their independent contributions would require a multivariate attribution framework and is left for future work.

The stronger climate-mode correlations in the western and central sectors relative to the east plausibly reflect connectivity and transport pathways. ENSO-related changes in ITF transport documented in Makassar, Lombok, and Timor passages imply that remotely forced pressure and flow anomalies can be communicated efficiently toward the western Java Sea [25, 26]. In contrast, the larger seasonal amplitude and deeper JJA minimum in the east are consistent with a more locally wind-dominated regime aligned with the regional geometry and upwelling patterns [16, 17].

Validation against tide gauges shows high correlations and modest errors at daily scales, supporting the use of gridded altimetry as a basin proxy in this research. Residual mismatches near harbours are expected, given complex coastal settings and sub-grid processes [27]. Monthly aggregation and detrending (standard practice to isolate seasonal and interannual variability from high-frequency noise and longer-term trends) helped to stabilize our diagnostics. In this research, confidence intervals around correlations and CCFs indicate that all reported peaks are statistically distinct from zero, while rapid decay away from the peak (especially for DMI) supports the interpretation of limited memory at monthly lags. Collectively, these checks suggest that the inferred signs, timing, and spatial contrasts are robust to known data limitations.

From an operational perspective, the sign and lag structure has potential to inform seasonal guidance: during forecasted IOD-positive conditions, expect suppressed sea level basin-wide (near-synchronous), while La Niña-like/positive SOI implies elevated sea level with ~1-month lead time, information that could be assimilated into seasonal advisories for port operations, navigation under under-keel constraints, and compound-flood risk when paired with storm surges and high tides.

Stronger process attribution would benefit from targeted diagnostics of wind stress and curl, and from regional/barotropic modeling experiments that partition local wind set-up from remotely forced pressure/transport anomalies, building on the established ENSO control of

Indonesian Throughflow (ITF) transports [25, 26]. Future work should also examine how these climate-mode signals translate into compound coastal hazard outcomes when combined with tides, surges, waves, and rainfall in key ports and low-lying coastlines of Java.

Conclusion

This study quantified the seasonal and interannual sea level variability in the Java Sea (2009–2024) and its links to the monsoon, ENSO (SOI), and the IOD (DMI), using DUACS altimetry validated against tide gauges. DUACS reproduces daily variability with high skill (median r ≈ 0.82; RMSE 5–11 cm; small negative biases), supporting its use as a basin proxy. Seasonally, sea level peaks in DJF, weakens in MAM, reaches a pronounced minimum in JJA, and recovers in SON, with clear zonal heterogeneity: the eastern Java Sea exhibits the strongest annual range (~18 cm) compared with the west/central sectors (~12–13 cm). The seasonal phase is non-synchronous, with W-JS maxima in May–June, E-JS in December–January, and C-JS behaving as a transition zone. Interannually, the IOD imprint is near-synchronous and negative (lag-0 , r ≈ −0.47 in W-/C-JS, −0.41 in E-JS), whereas the ENSO imprint peaks at lag +1 month (SOI leads; r ≈ 0.45–0.53), indicating higher sea level during La Niña and lower during El Niño. Beyond the Java Sea, these diagnostics illustrate how monsoon and climate teleconnections shape shelf sea-level variability across the Maritime Continent seas. While operational validation lies beyond this study, the established sign–lag relationships have potential to inform seasonal outlooks when integrated with local tide and surge information. Limitations include near-coastal retrieval challenges and our focus on variability rather than long-term trends or land subsidence. Future work should (i) partition local wind setup versus remote forcing with process-resolving models, (ii) address joint IOD–ENSO attribution using multivariate frameworks to isolate simultaneous effects, and (iii) integrate these drivers into compound coastal-hazard risk frameworks for ports and low-lying coasts.

Acknowledgment

The authors gratefully acknowledge the State College of Meteorology, Climatology, and Geophysics (STMKG) for funding and institutional support. Appreciation is also extended to the Indonesian Agency for Meteorology, Climatology, and Geophysics (BMKG) for providing access to the InaTNT tide-gauge dataset that underpinned the analyses. The views expressed are those of the authors and do not necessarily reflect those of STMKG or BMKG.

References

[1] S. Seftiani, I. A. P. Putri, I. Hidayati, L. K. Katherina, V. Ningrum, and D. Vibriyanti, "Climate change and COVID-19: The double whammy for coastal communities in Demak, Indonesia," in *IOP Conference Series: Earth and Environmental Science*, 2021.

[2] P. J. Ward, M. A. Marfai, F. Yulianto, D. R. Hizbaron, and J. C. J. H. Aerts, "Coastal inundation and damage exposure estimation: A case study for Jakarta," *Natural Hazards*, vol. 56, no. 3, pp. 899 – 916, 2011.

[3] A. Wicaksono and H. Herdiansyah, "The impact analysis of flood disaster in DKI Jakarta: Prevention and control perspective," in *Journal of Physics: Conference Series*, 2019.

[4] M. A. Marfai and L. King, "Potential vulnerability implications of coastal inundation due to sea level rise for the coastal zone of Semarang city, Indonesia," *Environmental Geology*, vol. 54, no. 6, pp. 1235 – 1245, 2008.

[5] L. Nurhidayah, "Sea-level rise (SLR) and its implication on human security and human rights in indonesia: A legal analysis," *Springer Climate*, pp. 33 – 52, 2021.

[6] K. Ichikawa, "Mean Seasonal Sea Surface Height Variations in and around the Makassar Strait," *Remote Sens (Basel)*, vol. 15, no. 17, 2023.

[7] A. Wirasatriya *et al.*, "Ekman dynamics variability along the southern coast of Java revealed by satellite data," *International Journal of Remote Sensing*, vol. 41, no. 21, pp. 8475 – 8496, 2020.

[8] E. Y. Handoko, L. K. Naibaho, D. Saptarini, and Yuwono, "Sea Level Variability around the Java Sea (study Area: Northern of Gresik and Surabaya) using Cryosat-2 Altimeter," in *IOP Conference Series: Earth and Environmental Science*, 2021.

[9] A. S. Delman, J. L. McClean, J. Sprintall, L. D. Talley, and F. O. Bryan, "Process-Specific Contributions to Anomalous Java Mixed Layer Cooling During Positive IOD Events," *Journal of Geophysical Research Oceans*, vol. 123, no. 6, pp. 4153 – 4176, 2018.

[10] T. F. Xu *et al.*, "Observed Water Exchange Between the South China Sea and Java Sea Through Karimata Strait," *Journal of Geophysical Research Oceans*, vol. 126, no. 2, 2021.

[11] G. Taburet *et al.*, "DUACS DT2018: 25 years of reprocessed sea level altimetry products," *Ocean Science*, vol. 15, no. 5, pp. 1207–1224, Sep. 2019.

[12] M. Passaro, Z. A. Nadzir, and G. D. Quartly, "Improving the precision of sea level data from satellite altimetry with high-frequency and regional sea state bias corrections," *Remote Sensing of Environment*, vol. 218, pp. 245 – 254, 2018.

[13] M. Pirooznia, M. R. Naeeni, and T. Yousefzadeh, "Point-wise determination of vertical deformation at southern coastal areas of Caspian sea by combination of satellite altimetry and tide gauge observations," *Annals of Geophysics*, vol. 63, no. 6, pp. 1 – 19, 2020.

[14] Husnayaen *et al.*, "Physical assessment of coastal vulnerability under enhanced land subsidence in Semarang, Indonesia, using multi-sensor satellite data," *Advances in Space Research*, vol. 61, no. 8, pp. 2159 – 2179, 2018.

[15] C. E. J. van Bijsterveldt *et al.*, "Subsidence reveals potential impacts of future sea level rise on inhabited mangrove coasts," *Nature Sustainability*, vol. 6, no. 12, pp. 1565–1577, Dec. 2023.

[16] A. Wirasatriya, R. D. Susanto, K. Kunarso, Abd. R. Jalil, F. Ramdani, and A. D. Puryajati, "Northwest monsoon upwelling within the Indonesian seas," *International Journal of Remote Sensing*, vol. 42, no. 14, pp. 5437 – 5458, 2021.

[17] H. A. Rachman *et al.*, "Dynamics of upwelling variability in the southern Indonesia region revealed from satellite data: Role of ENSO and IOD," Journal of Sea Research, vol. 202, 2024.

[18] R. Y. Setiawan, A. Wirasatriya, U. Hernawan, S. Leung, and I. Iskandar, "Spatio-temporal variability of surface chlorophyll-a in the Halmahera Sea and its relation to ENSO and the Indian Ocean Dipole," *International Journal of Remote Sensing*, vol. 41, no. 1, pp. 284 – 299, 2020.

[19] R. D. Susanto and R. D. Ray, "Seasonal and Interannual Variability of Tidal Mixing Signatures in Indonesian Seas from High-Resolution Sea Surface Temperature," *Remote Sensing*, vol. 14, no. 8, 2022.

[20] E. Y. Handoko, H. Hariyadi, and A. Wirasatriya, "The ENSO's Influence on the Indonesian Sea Level Observed Using Satellite Altimetry, 1993 - 2016," in *Proceedings - 2018 IEEE Asia-Pacific Conference on Geoscience, Electronics and Remote Sensing Technology: Best Practice for Disaster Mitigation using Geoscience, Electronics, and Remote Sensing, AGERS 2018*, 2018.

[21] E. Y. Handoko, D. S. Richasari, and D. G. Pratomo, "Seasonal and Interannual Variability of Sea Level in the Indonesian Seas using Satellite Altimetry," in *IOP Conference Series: Earth and Environmental Science*, 2021.

[22] A. Nurlatifah, Martono, I. Susanti, and M. Suhermat, "Variability and trend of sea level in southern waters of Java, Indonesia," *Journal of Southern Hemisphere Earth Systems Science*, vol. 71, no. 3, pp. 272 – 283, 2021.

[23] A. Fadlan, D. N. Sugianto, Kunarso, and M. Zainuri, "Influence of ENSO and IOD on the Variability of Sea Surface Height in the North and South of Java Island," in *IOP Conference Series: Earth and Environmental Science*, 2017.

[24] R. Rachmayani, N. S. Ningsih, F. Hanifah, and Y. Nabilla, "Long-Term Trend and Variability of Volume Transport and Advective Heat Flux through the Boundaries of the Java Sea Based on a Global Ocean Circulation Model (1950–2013)," *Water (Switzerland)*, vol. 15, no. 4, 2023.

[25] F. Jamil, Sakka, and D. Berlianty, "ENSO impacts during west and east monsoon to the ocean current and water mass characteristics in the Makassar Strait," in *IOP Conference Series: Earth and Environmental Science*, 2019.

[26] N. A. Fekranie, A. Setiawan, and M. R. Putri, "Variability of Indonesian Throughflow Transport in the Indonesian Seas during Triple-Dip la Niña," in *IOP Conference Series: Earth and Environmental Science*, 2024.

[27] L. A. Ruiz Etcheverry, M. Saraceno, A. R. Piola, G. Valladeau, and O. O. Möller, "A comparison of the annual cycle of sea level in coastal areas from gridded satellite altimetry and tide gauges," *Continental Shelf Research*, vol. 92, pp. 87–97, 2015.